

An HF-Radar Test Deployment Amidst an ADCP Array on the West Florida Shelf

F. J. Kelly, CBI
J. S. Bonner, CBI
J. C. Perez, CBI
J. S. Adams, CBI
D. Prouty, CBI
D. Trujillo, CBI

R. H. Weisberg, USF
M. E. Luther, USF
R. He, USF
R. Cole, USF
J. Donovan, USF
C. R. Merz, USF

Conrad Blucher Institute
for Surveying and Science,
Texas A&M University-Corpus Christi
6300 Ocean Drive
Corpus Christi, Texas, 78412, USA

College of Marine Science,
University of South Florida,
140 7th Avenue South,
St. Petersburg, Florida, 33701, USA

Abstract- For 11 days in January 2001, the Conrad Blucher Institute for Surveying and Science, Texas A&M University-Corpus Christi, in collaboration with the College of Marine Science, University of South Florida, deployed a pair of 25-MHz CODAR Ocean Systems HF-Radars on the West Florida Shelf over an array of six acoustic Doppler current profilers. The radar footprint had a maximum range of 60 km offshore, and it included mooring locations between the 10 m to 30 m isobaths. We examine, using a variety of metrics, the correlation between the surface currents measured remotely by the HF-Radar and the subsurface currents measured by the ADCP's, which were either bottom- or surface buoy-mounted. Qualitative comparisons are generally good for this inner-shelf environment where the wind-driven current magnitudes were less than about 40 cm/s. The scalar regression analysis shows correlation coefficients (R) of 0.8 to 0.9 for the alongshelf components but 0.6 or less for the cross-shelf components. Complex vector correlation produces correlation values of 0.76 to 0.90 and a consistently clockwise veering from the radar-measured currents to the ADCP-measured ones ranging from of 1.3° to 5.2° . The alongshelf surface currents measured by the radar are about 30% larger than those of the ADCPs measured 2 to 3 m below the surface according to standard deviations and linear regression slopes.

I. INTRODUCTION

During 2000, the Conrad Blucher Institute for Surveying and Science (CBI) at Texas A&M University-

The HF-Radar portion of this work was supported by the Texas General Land Office under the Interagency Cooperation Contracts 00-43R and 02-115R. The USF investigators acknowledge support from the Office of Naval Research, Grant #N00014-98-1-0158 and the National Oceanic and Atmospheric Administration, Grant #NA76RG0463.

Corpus Christi and the Texas Engineering Experiment Station (TEES) acquired a pair of SeaSonde® 25-MHz HF-Radar systems from CODAR Ocean Sensors for use in oil-spill response research. These radar systems are designed to map the surface current flow over a pre-determined spatial grid at regular intervals of time. They can also provide measurements of wave height, period and direction, and wind direction.

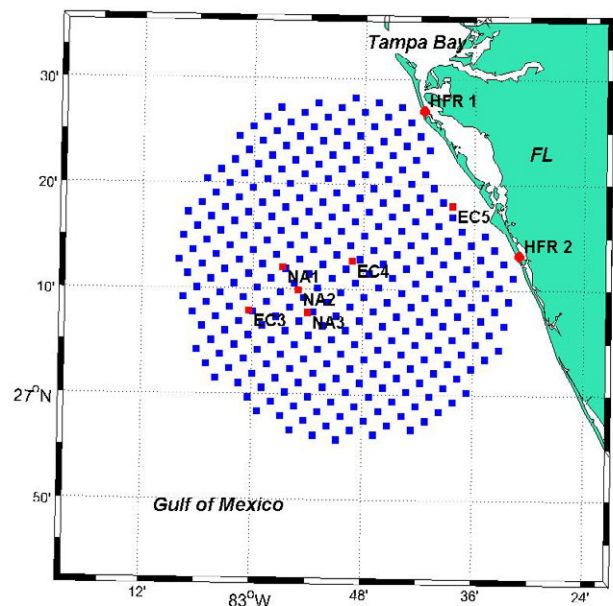


Fig. 1. Map showing coverage grid of the HF-Radar, the two Radar sites, and the six USF mooring locations. The solid HF-Radar grid points are those for which the angle of intersection of the radials from the two sites is greater than 30° and less than 150° .

For mobility, ease of setup, and operation in the Gulf coast environment, the SeaSondes were installed in small trailers, complete with generator power and air conditioning. A series of deployment exercises were conducted to gain operational experience under various conditions on both bays and coastal waters. CBI is the only SeaSonde user currently operating its systems in a truly mobile mode (D. Barrick, personal communication). In this paper, we describe the results from an exercise in January 2001 in collaboration with the College of Marine Science at the University of South Florida (USF), which was operating six ADCP current-meter sites off the West Florida coast south of Tampa Bay (Fig. 1).

Over the past fifty years, researchers have developed the underlying techniques that are used to extract water current measurements from the Doppler shift of the Bragg scattered radar return signal or sea echo [1] [2] [3] [4]. Present current-mapping radar systems are differentiated principally by their method of bearing determination—phased array or direction finding [4] [5]. The COS SeaSonde falls in the latter category, using a three-element, crossed-loop, monopole receive antenna and software direction-finding algorithms [6] [7]. Regardless of system design, the current-mapping radar is becoming an accepted oceanographic tool, and it is important to compare its measurements with those from more conventional instruments in order to provide perspective on what is being measured. For example, in this experiment, the surface current at a radar grid point represents a depth integral over the top 0.5 m of the water column, spatially averaged over a circular area of 4.5 km radius and temporally averaged over sixty minutes. The corresponding bottom-mounted ADCP measurement at the top bin in 20-m water depth represents a depth integral over one meter at a depth 2.5 m below the surface, spatially sampled over 13-m radial area, and temporally burst sampled for six minutes each hour. Thus, the general contrasting characteristics of the two instruments are that the radar yields a spatially and temporally averaged surface current measurement while the ADCP produces a subsurface point measurement. Nevertheless, one would hope for reasonably comparable results, and indeed, other studies using somewhat different instrument configurations have found good comparisons [5]. In this paper, we examine the correlations between the currents measured by the SeaSonde HF-Radar system and the ADCPs using a variety of metrics and explore the observed differences.

II. THE EXPERIMENT

CBI deployed its mobile trailers containing the HF-Radars on the beaches at Anna Maria Key (HFR1) and Siesta Key (HFR2) as shown in Fig. 1, yielding a baseline distance of 19.7 km. The availability of commercial power eliminated the need for generators. For example, the trailer at HFR1 was located next to a lifeguard tower (Fig. 2) on Coquina Beach. The transmitter and receiver antennas were placed about 20 and 32 m to the south, respectively, (to the left in Fig. 2, but not shown) and about 30 m from the water. The setup at HFR2 was similar. Table I

provides details of the setup parameters for both sites. For this deployment, the actual antenna patterns were not measured, and all computations relied on ideal antenna patterns. However, the antennas at both sites were located on broad flat beaches with no near-field obstacles.



Fig 2. Picture of the HF-Radar trailer at HFR1, next to a Lifeguard tower. The transmit and receive antennas (not shown) were located about 80 m to the south (left) of the trailer

TABLE I
SEASONDE HF-RADAR CONFIGURATION PARAMETERS AND SPECIFICATIONS

SITE CONFIGURATION PARAMETERS		
	HFR1	HFR2
Latitude	27.2207° N	27.4498° N
Longitude	82.5182° W	82.6927° W
Operating Frequency	26.180 MHz	25.250 MHz
Water Wave Length	5.73 m	5.94 m
SEASONDE SPECIFICATIONS		
Baseline Separation of Sites	19.7 km	
Modulation Format	Pulsed Swept Frequency CW	
Sweep Repetition Frequency	2 Hz	
Blanking Distance (Max Range)	486.4 μ s or 72.9 km	
Polarization	Vertical	
Number of Valid Measurement Cells	312	
Range Cell Resolution	3 km	
Measurement Cycle	60 minutes	
Measured Radiated Power	32 Watts avg.	
Angular Resolution	5°	
Map Vector Current Accuracy	< 7 cm s ⁻¹	
Map Vector Direction Accuracy	< 10°	
Measurement Depth	0.5 m @ 26 MHz	

The HF-Radar system produced a total of 269 hourly surface current maps from 1600 UTC January 20 through 2000 UTC January 31, 2001 on a 3 km x 3 km grid. The initial rectangular grid contained 20 points perpendicular to the baseline between HFR1 and HFR2 and 21 points parallel to it, beginning 3 km seaward from it, for a total of 420 points. A geometrical constraint (the Geometrical Dilution Of Precision, or GDOP) requires that the angle of intersection of radial lines from each radar site be greater than 30° and less than 150°. Applying this condition yields a useful domain of 312 grid points, as shown in Fig. 1. In subsequent discussions, we refer to a grid point by its baseline-perpendicular and baseline-parallel indices [i, j] from the original rectangular grid, e.g., HFR[8,11], where HFR[1, 1] lies at the southeast corner (not shown in Fig. 1 because of the GDOP constraint). The maximum range the radar is limited by the blanking time. Initially, this parameter was set to 243.2 μ s or 36.5 km, which is just short of the USF moorings NA1, NA2 and NA3 (Fig. 1). At 0025 UTC January 26, 2001, about midway through the experiment, the blanking time was doubled, yielding a maximum range of 73 km and the grid shown in Fig. 1.

The HF-Radar coverage area was centered on an existing operational array of six ADCP sites (Fig. 1). Table II presents the various combinations of mooring and instrument configurations employed during the period of this experiment. Note that three of the sites EC4, EC5, and NA1, were bottom-mounted, with up-looking Broadband ADCPs. The other three sites NA2, NA3, and EC3, were surface moorings with down-looking ADCPs mounted in 2.5-m diameter discus-type bouys. The ADCPs in NA2 and NA3 were Narrowband units, while that in EC3 was a Broadband unit. In this comparison study, we use only the topmost useable bin of data from each ADCP.

Winds during the study were consistent with climatologic data for the region [8] [9]. During the first seven days (January 20-26) strong northwesterly (up to 12 ms^{-1}) and weaker northeasterly winds prevailed. A three-day transition period of weak and variable winds was followed by a switch to persistent southeasterly and southerly winds of about 5 ms^{-1} beginning on January 29th. HF-Radar surface current maps before and after the wind shift are shown in Fig. 3. As might be expected, the coastal current patterns correspond to the direction and magnitude of wind forcing, with near shore waters responding more quickly to shifts in wind direction.

TABLE II
CONFIGURATION PARAMETERS FOR ADCP INSTRUMENTS DEPLOYED BY USF. ALL HAD 20° TRANSDUCER HEADS. ALL WERE CONFIGURED WITH 6-MINUTE BURST SAMPLES OF 360 PINGS BEGINNING AT THE TOP OF THE HOUR. THE DEPTHS OF THE TOP BIN FOR THE BOTTOM-MOUNT, UPWARD LOOKING INSTRUMENTS WERE COMPUTED USING A MEASURED WATER DEPTH AND A DISTANCE FROM THE BOTTOM FOR EACH BIN. THE DEPTHS OF THE TOP BIN FOR THE SURFACE BUOYS ARE ACTUAL WATER DEPTH.

Site	EC3	EC4	EC5
Workhorse Model	300 kHz BB	300 kHz BB	600 kHz BB
Water Depth	30m	20m	10m
Top Bin Depth	3.5m	2.5m	2.0m
Bin size	1.0m	0.5m	0.5m
Orientation	Down	Up	Up
Mooring type	Surface	Bottom-mount	Bottom-mount
Latitude	27.1310	27.2112	27.2987
Longitude	-83.0059	-82.8206	-82.6389

Site	NA1	NA2	NA3
Workhorse Model	300 kHz BB	600 kHz NB	600 kHz NB
Water Depth	25m	25m	25m
Top Bin Depth	2.5m	3.0m	3.0m
Bin size	0.5m	1.0m	1.0m
Orientation	Up	Down	Down
Mooring type	Bottom-mount	Surface	Surface
Latitude	27.2005	27.1645	27.1290
Longitude	-82.9458	-82.9168	-82.9001

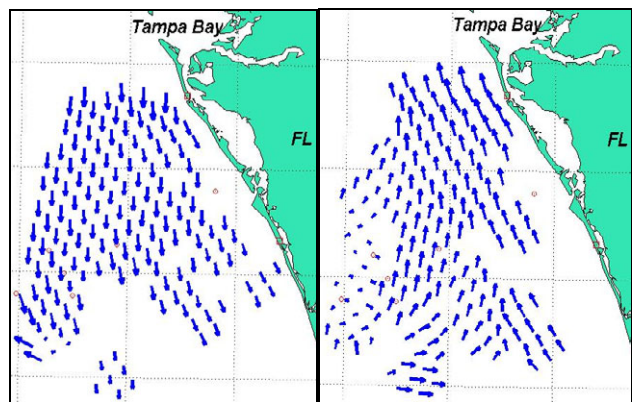


Fig 3. Surface current maps for 1/26/01 0600 UTC and 1/31/01 0500 UTC, showing current reversal after frontal passage

III. RESULTS

Currents in near-coastal regions are strongly steered by the topography, and the angle of the principal axis tends to parallel the coast. Therefore, time series of coastal currents are normally discussed in terms of a rotated coordinate system, with components parallel and perpendicular to the local topography. In this study, we did not use a single angle of rotation for all time series of current velocity because potential bias errors in direction determination would bias the generally smaller cross-shelf component with along-shelf current variance. Instead, we performed a principal component analysis on each velocity time series and rotated it to the directions of the major and minor axes of its variance ellipse to obtain the most linearly independent orthogonal components for that series [10]. The analysis was done on a pair-by-pair basis using only the common good points. The results are shown in Table 3, which includes the number of common good points, the angle from north of the major axis, and the magnitude of the major and minor axes in variance units (cm^2s^{-2}). In all subsequent analyses and discussion the term along-shelf refers to the component parallel to the major axis of a specific vector time series.

TABLE III
RESULTS OF THE PRINCIPLE AXIS ANALYSIS OF EACH VECTOR TIME SERIES: ANGLE OF MAXIMUM VARIANCE RELATIVE TO TRUE NORTH, MAJOR AXIS (VARIANCE) OF PRINCIPLE ELLIPSE AND MINOR AXIS (VARIANCE) OF PRINCIPLE ELLIPSE

Current Meter	Number Pts.	Angle ($^{\circ}$ True)	Major Axis (cm^2s^{-2})	Minor Axis (cm^2s^{-2})
EC5	67	158.7	13.2	3.5
HFR [2 11]	67	154.8	16.2	5.4
EC4	207	154.9	11.3	6.0
HFR [8 11]	207	156.8	17.1	5.0
NA1	146	167.8	11.9	6.4
HFR [10 13]	146	161.4	16.8	5.0
NA2	128	166.4	13.3	6.2
HFR [10 11]	128	161.0	18.8	4.8
NA3	114	162.9	11.6	5.0
HFR [10 10]	114	165.6	17.5	4.5
EC3	90	169.6	11.7	5.4
HFR [11 12]	90	167.6	16.0	5.9

Vector time-series plots of the currents measured at EC4 and the closest radar grid point HFR[8 11] are shown in Fig. 4. Of the six pairs of current measurements considered here, this one has the largest number of common good points (Table III). The corresponding graphs of along-shelf and cross-shelf components are shown in Fig. 5. The two figures illustrate the characteristics of the two types of instruments noted earlier. The radar currents are “smoother” than those from the ADCP because of the greater spatial and temporal averaging, and for this shallow, near shore location, the radar-measured surface currents (top 0.5 m) are somewhat stronger than those from the top 0.5-m ADCP bin located 2.5 m below the surface. The time-series plots also show the reversal in along-shelf flow that began about January 28th.

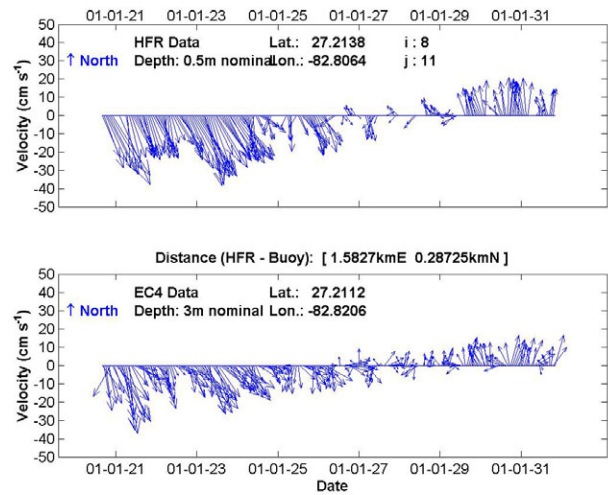


Fig. 4. Time-series vector plots of currents observed by the HF-Radar at grid point [8 11] (upper) and the ADCP at 3 m below the surface at mooring EC4 (lower).

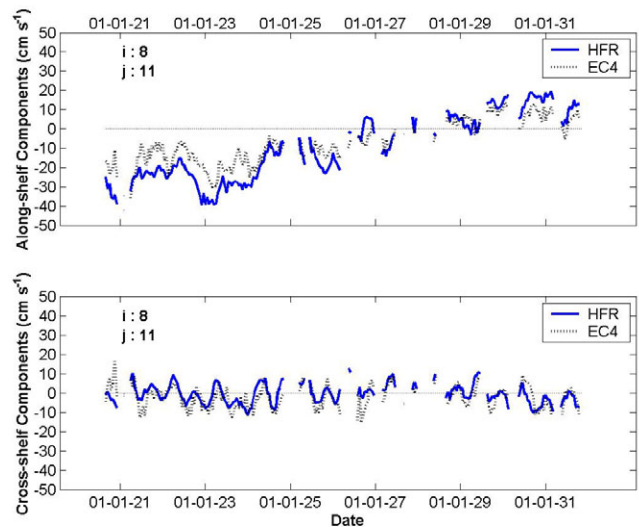


Fig. 5. HFR[8 11] vs. EC4 time-series plots for alongshelf (upper) and cross-shelf components (lower), showing only common good points.

Following the rotation of each vector series into the axes of its variance ellipse, we used linear regression and basic statistics to compare the alongshelf and cross-shelf components rather than spectral time-series analysis methods because of the short record lengths and data gaps. The “standard” linear least-squares fitting assumes the abscissa values are error free and well known, which is not true for this study. Here, there are uncertainties in both coordinates that we assume to have approximately equal weights, and we used the more general algorithms that allow for some uncertainties in both co-ordinates [10] [11] [12] [13]. When the errors in both co-ordinates are equally weighted, the best-fit line is that which minimizes the sum of the squares of the perpendicular distance of the points from the line [10]. A representative scatter plot and its regression line are shown in Fig. 6 for the time series shown in Figs. 4 and 5. Results of all regressions are summarized in Table IV, and the basic statistics for each time series component are shown in Table V. Following the method of Kundu [14], we also estimated the degree of correlation, γ , and the veering, θ , between the vector time series (Table VI).

We first examine the alongshelf basic statistics for the pairs, starting with the ADCP/radar grid-point pair closest to the coast, EC5/HFR[2 11]. The surface radar current shows slightly stronger along-shelf flow in the mean, range and standard deviation; but note there are only 67 common good points. For the EC4/HFR[8 11] pair the radar currents are also stronger. Small differences visible at some points in the time-series plots (Figs 4 and 5) are masked by the averaging process. The radar coverage did not quite reach the ADCP moorings farther offshore (NA1, NA2, NA3 and EC3) during the first half of the experiment. For statistical comparison we choose radar grid points located 6 to 12 km shoreward of these moorings (Table IV) in order to have longer corresponding radar time series. ADCP mean values for these pairs are about 5 cm s^{-1} stronger (downcoast) than the radar means. The reason is that the range of the values for the ADCP-measured flows (min to max) are shifted about 15 cm s^{-1} towards the negative (downcoast) compared to the radar data, which in turn suggests that the wind-driven shift to upcoast flow observed in the radar surface currents was not seen as quickly and as strongly at the depths of the top ADCP bins. Standard deviations for the radar time series are larger than those for the ADCPs by about 3 to 6 cm s^{-1} for all pairs, and all slopes from the linear regression analyses of the alongshelf components are positive and on the order of 0.7, i.e., higher radar values (Table IV and Fig. 6). Together, these metrics indicate that the alongshelf surface currents measured by the radar are stronger than those of the ADCPs by about 30%. Cross-shelf statistics on a pair-by-pair basis are almost identical for all six pairs, and the means and standard deviations are small, i.e., on the order of 3 and 6 cm s^{-1} , respectively.

Linear regression between alongshelf components of the ADCP/HFR time-series pairs yields generally high correlation coefficients (Table IV). At the two pairs closest to the coast R-values exceed 0.9, and at three of the pairs farther offshore they are about 0.8. The cross-shelf components are poorly correlated in all cases, with R-

values of 0.6 or less. The complex vector correlation coefficients (Table VI) are consistent with the scalar alongshelf correlation coefficients: they are highest for the pairs nearest the coast, and exceed 0.76.

Both the principal axis analysis (Table III) and the complex vector correlation (Table VI) provide estimates of the directional differences between the pairs. As might be expected, the magnitudes of the directional differences are small, i.e., 1° to 6° . The complex vector correlation produces a consistently clockwise veering, but the orientations of the principal axes provide no consistent relative directional rotation. As the ADCP measures approximately 2m to 3m deeper than the HFR, the rotation angles indicated by the complex vector correlation are consistent with the combined Ekman-geostrophic response of the West Florida Shelf coastal currents to wind forcing [15]. We also note that the orientations of the principal axes for all pairs show a consistent increasing angle relative to north, i.e., from about 155° to about 168° , moving from the shallower to the deeper sites.

TABLE IV
REGRESSION RESULTS: SLOPE, INTERCEPT AND CORRELATION COEFFICIENT FOR GIVEN ADCP/HF-RADAR GRID-POINT PAIR, AND THE RANGE AND BEARING FROM THE ADCP TO THE RADAR GRID POINT.

Regression	Slope	Intercept (cm s^{-1})	Correlation Coefficient (R)	Range (km) & Bearing ($^\circ$ T)
EC5 vs. HFR [2 11]				1.8 292
Alongshelf	0.82	-0.88	0.92	
Cross shelf	0.64	1.9	0.57	
EC4 vs. HFR [8 11]				1.4 78
Alongshelf	0.66	-0.57	0.93	
Cross shelf	1.2	1.2	0.62	
NA1 vs. HFR [10 13]				6.3 60
Alongshelf	0.71	-8.6	0.61	
Cross shelf	1.3	2.3	0.55	
NA2 vs. HFR [10 11]				6.3 71
Alongshelf	0.71	-7.8	0.81	
Cross shelf	1.3	-1.3	0.62	
NA3 vs. HFR [10 10]				7.0 59
Alongshelf	0.66	-6.5	0.79	
Cross shelf	1.1	-1.8	0.53	
EC3 vs. HFR [11 12]				12.5 58
Alongshelf	0.73	-6.7	0.81	
Cross shelf	0.91	0.33	0.61	

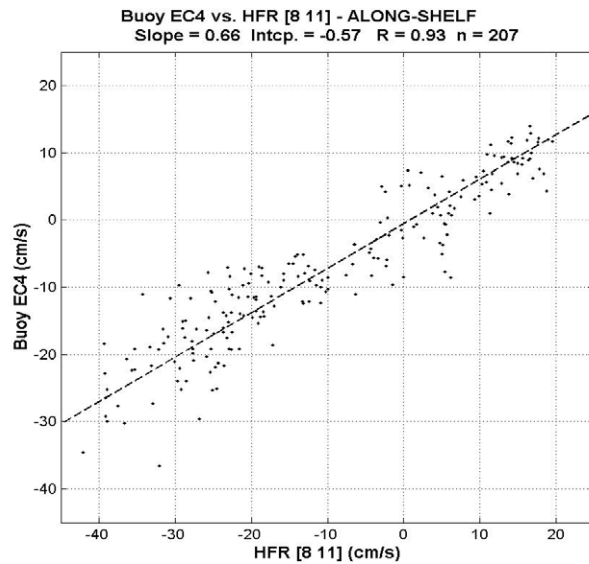


Fig. 6. Scatter plot and linear regression of alongshelf components of EC4 vs. HFR[8 11]. Slope = 0.66, intercept = -0.57 cm s^{-1} , correlation coefficient $R = 0.93$.

TABLE V

BASIC STATISTICS FOR EACH SERIES COMPONENT. “N” IS NUMBER OF GOOD POINTS IN COMMON FOR THE GIVEN PAIR. MINIMUM, MAXIMUM AND STANDARD DEVIATION HAVE UNITS CM S^{-1} . POSITIVE VALUES ARE UCOAST AND OFFSHORE.

Series	N	Mean	Min.	Max.	Std.
Along-shelf					
EC5	67	-12.7	-31.8	18.0	13.2
HFR [2 11]	67	-14.5	-38.9	18.9	16.2
EC4	207	-7.5	-36.5	14.0	11.3
HFR [8 11]	207	-10.5	-42.1	19.6	17.1
NA1	146	-18.6	-52.5	2.4	11.9
HFR [10 13]	146	-14.2	-54.4	15.4	16.8
NA2	128	-15.4	-57.0	5.4	13.3
HFR [10 11]	128	-10.7	-45.4	21.4	18.8
NA3	114	-10.6	-48.9	10.7	11.6
HFR [10 10]	114	-6.1	-37.3	24.3	17.5
EC3	90	-10.6	-37.0	5.5	11.7
HFR [11 12]	90	-5.4	-44.5	20.7	16.0
Cross shelf					
EC5	67	-1.3	-10.6	6.4	3.5
HFR [2 11]	67	1.0	-9.1	12.2	5.4
EC4	207	-2.1	-14.5	16.4	5.9
HFR [8 11]	207	-0.7	-11.5	12.7	5.0
NA1	146	-4.5	-19.9	13.3	6.4
HFR [10 13]	146	-1.8	-11.1	12.5	5.0
NA2	128	-2.6	-16.7	14.4	6.2
HFR [10 11]	128	-3.0	-12.0	9.8	4.8
NA3	114	-1.4	-14.6	11.0	5.0
HFR [10 10]	114	-2.9	-12.2	14.1	4.5
EC3	90	-2.1	-14.7	10.5	5.4
HFR [11 12]	90	-2.0	-14.3	12.7	5.9

TABLE VI

COMPLEX CORRELATION COEFFICIENTS, γ , AND THE ROTATION ANGLE, θ , FOR THE HFR AND ADCP CURRENT VELOCITIES. POSITIVE THETA INDICATES THAT THE ADCP CURRENTS ARE ROTATED CLOCKWISE LOOKING DOWN FROM THOSE OF THE RADAR.

Pair	γ	θ
HFR [2 11] vs. EC5	0.90	2.5
HFR [8 11] vs. EC4	0.87	5.1
HFR [10 13] vs. NA1	0.62	11.3
HFR [10 11] vs. NA2	0.78	1.3
HFR [10 10] vs. NA3	0.76	5.2
HFR [11 12] vs. EC3	0.79	5.2

IV. CONCLUSIONS

We compared surface currents measured remotely by high frequency radar with subsurface currents measured at fixed locations by ADCPs moored on the west Florida continental shelf between the 10 m and 30 m isobaths. Qualitative comparisons over the approximate 11-day radar deployment are generally good for this inner-shelf environment where the wind-driven current magnitudes were less than about 40 cm/s. Quantitative comparisons using scalar regression analysis shows correlation coefficients (R) of 0.8 to 0.9 for the alongshelf components but 0.6 or less for the cross-shelf components. Complex vector correlation produces correlation values of 0.76 to 0.90 and a consistently clockwise veering from the radar-measured currents to the ADCP-measured ones ranging from of 1.3° to 5.2° . The alongshelf surface currents measured by the radar are about 30% larger than those of the ADCPs measured 2-3 m below the surface according to standard deviations and linear regression slopes. Whether these quantitative differences result from instrument errors, sampling differences, or natural variability remains to be determined. They are generally within the instrument errors. Sampling resolutions by radar and point measurements are inherently different (averages over about 4 km versus over tens of meters, and nature does exhibit time and space variable current shear over the upper few meters of the water column). These short duration comparisons at least yield encouraging results on the use of surface radars for mapping WFS current fields. Longer-term deployments will allow for decomposing the observations into tidal and wind-forced synoptic portions with sufficient degrees of freedom to better quantify the differences between measurement techniques and their possible origins.

ACKNOWLEDGMENTS

We thank the Texas General Land Office and Ms. Robin Jamail for their encouragement and support. The USF investigators thank the Office of Naval Research and the National Oceanic and Atmospheric Administration for their support and encouragement. Thanks also to CBI personnel James Rizzo, Terry Riggs and Drew Maczko for their assistance in the mobilization and operation of the radar sites. Dr. Dana Wetzel of Mote Marine Aquarium provided invaluable assistance in locating sites for the radars. We also thank Mr. Jason Iott at the Gulf Beach Campground in Siesta Key for providing an ideal location for the equipment at the HFR2 site, and we thank the Manatee County Parks Department for permitting the HFR1 site to be setup at a lifeguard tower on Coquina Beach, Anna Maria Key.

REFERENCES

- [1] D. Crombie, "Doppler spectrum of sea echo at 13.56 Mc/s," *Nature*, vol. 175, pp. 681-682, 1955.
- [2] D. Barrick, "First-order theory and analysis of MF/HF/VHF scatter from the sea," *IEEE Transactions on Antennas and Propagation*, vol. AP-20, no. 1, pp. 2-10, January 1972.
- [3] D. Crombie, "Resonant backscatter from the sea and its application to physical oceanography", *IEEE International Conference Proceedings on Engineering in the Ocean environment*, pp 174-179, 1972.
- [4] C. Teague, J. Vesecky, and D. Fernandez, "HF Radar Instruments, Past to Present," *Oceanography*, vol. 10, no. 2, pp. 40-44, 1997.
- [5] L. Shay, T. Cook, H. Peters, A. Mariano, R. Weisberg, P. An, A. Soloviev, and M. Luther, "Very high-frequency radar mapping of surface currents," *IEEE J. of Oceanic Eng.*, vol. 27, no. 2, pp. 155-169, April 2002
- [6] B. Lipa, and D. Barrick, "Least-squares methods for the extraction of surface currents from CODAR crossed-loop data: Application at Arsløe," *IEEE J. of Oceanic Eng.*, vol. OE-8, no. 4, pp 226-253, October 1983.
- [7] D. Barrick, and B. Lipa, "Evolution of bearing determination in HF current mapping radars," *Oceanography*, vol. 10, no. 2, pp. 72-75, 1997.
- [8] R. Weisberg, B. Black, and H. Yang, "Seasonal modulation of the West Florida continental shelf circulation," *Geophys. Res. Letters*, vol. 23, no. 17, pp. 2247-2250, August 1996.
- [9] H. Yang, and R. Weisberg, " Response of the West Florida Shelf circulation to climatological wind stress forcing," *J. Geophys. Res.*, vol. 104, pp. 5301-5320, March 1999.
- [10] W. Emery, and R. Thomson, *Data Analysis Methods in Physical Oceanography*. Pergamon, 634 pp., 1998.
- [11] B. Reed, "Linear least-squares fits with errors in both coordinates. II: Comments on parameter variances," *Am. J. Phys.*, vol. 60, no. 1, 1992.
- [12] B. Reed, "Linear least-squares fits with errors in both coordinates," *Am. J. Phys.*, vol. 57, no. 7, 1989.

- [13] P. Sprent, and G. Dolby, "The geometric mean functional relationship," *Biometrics*, vol. 36, pp. 547-550, 1980.
- [14] P. Kundu, "Ekman veering observed near the bottom," *J. Phys. Oceanogr.*, vol. 6, no. 2, pp. 238-242, 1976.
- [15] R. Weisberg, B. Black, and Z. Li., "An upwelling case study on Florida's west coast," *J. Geophys. Res.*, vol. 105, pp. 11459-11469, 2000.

DISCLAIMER

This paper does not necessarily reflect the views or policies of the Texas General Land Office, Texas A&M University, Texas A&M University-Corpus Christi, the University of South Florida, or the other agencies providing financial and service support. Mention of trade names or commercial products does not constitute a commercial endorsement or recommendation for use.